On the Non-Equilibrium Behavior of Fuel-Rich Hydrocarbon/Air Combustion Within Perfectly Stirred Reactors

Cesar Celis, Luis Fernando Figueira da Silva

On the Non-Equilibrium Behavior of Fuel Rich Hydrocarbon/Air Combustion within Perfectly Stirred Reactors

Cesar Celis†, Luís Fernando Figueira da Silva

Department of Mechanical Engineering, Pontifícia Universidade Católica do Rio de Janeiro
Rua Marquês de São Vicente 225, Rio de Janeiro, RJ 22451-900, Brazil

† Corresponding author – Tel.: +55 21 3527 1641
E-mail address: Cesar.Celis@PUC-Rio.br (C. CELIS)

On the Non-Equilibrium Behavior of Fuel Rich Hydrocarbon/Air Combustion within Perfectly Stirred Reactors

The origins of non-equilibrium behavior observed, even for relatively large residence times, in perfectly stirred reactors (PSRs) burning fuel rich mixtures, are addressed. These PSR deviations from chemical equilibrium are characterized by using PSR-based results of CO/O2 reacting mixtures. Accordingly, the origins of the PSR non-equilibrium behavior are elucidated by (i) analyzing the relevance of the reaction steps involved in the CO/O2 kinetic mechanism, (ii) deriving and assessing analytical expressions reproducing the PSR results, and (iii) examining asymptotic limit solutions emphasizing a possible cause of the non-equilibrium behavior observed. The main results highlight that the PSR non-equilibrium behavior is controlled by a competition between (i) the rate of progress variable backward component of the CO + O + M ⇌ CO2 + M reaction and (ii) the ratio between the reactor inlet O2 molar concentration and the reactor residence time. Thus, even when the reactor is operating in a region of temperature invariance (plateau), where chemical equilibrium conditions could be presumed, there are some chemical species, such as O2 and O, whose steady state does not correspond to that of chemical equilibrium. It is concluded then that particular attention should be paid when analyzing PSR results, obtained at relatively high mixture equivalence ratios, which may not correspond to equilibrium, in situations where it could be presumed to happen so. A brief discussion on the extent of such non-equilibrium phenomena is performed as well using more complex syngas/O2 mixtures.

Keywords: Perfectly stirred reactors, Non-equilibrium behavior, Fuel rich mixtures.

1 Introduction

In perfectly stirred reactors (PSRs) (Longwell and Weiss, 1955), or well stirred reactors (WSRs) as sometimes are referred to (Williams, 1985; Turns, 2000), it is assumed that the fuel and oxidant streams entering the reactor are instantaneously and perfectly mixed with the combustion gases already present within the reactor. The exit

stream is then representative of the homogeneous reactor composition. Even though PSRs have been around for more than six decades, they are still widely used to model combustion processes. They are employed, for instance, in (i) the study or derivation of detailed (Le Cong and Dagaut, 2007; Le Cong and Dagaut, 2008) and reduced (Mallampalli et al., 1998; Sung et al., 2001; Nikolaou et al., 2013) chemical kinetic mechanisms, (ii) the prediction of pollutant formation (Fichet et al., 2010; Amzin and Cant, 2015; Adhikari et al., 2016), (iii) ignition and extinction phenomena analyses (Snegirev, 2015; Snegirev and Tsoy, 2015), and (iv) reactor networks used to describe practical combustion systems (Celis et al., 2009; Orbegoso et al., 2011; De Tony et al., 2013).

Classical PSR analysis/theory (Williams, 1985; Turns, 2000; Zeldovich et al., 1985; Glassman and Yetter, 2008) is developed either (i) to analytically derive critical times considering a single chemical reaction – where thermochemical equilibrium is always attained as reactor residence time tends to infinity; or (ii) to numerically investigate extinction in lean to stoichiometric conditions using detailed chemistry. The infinitely fast mixing of reactants and products hypothesis leads to a situation where the residence time is the only time scale competing with the chemical reactions characteristic time (Sung et al., 2001). Consequently, for adiabatic conditions, PSR properties are generally expected to approach to those characterizing (i) chemical equilibrium, for large reactor residence times; and (ii) extinction (where chemical reactions can no longer be sustained), for small ones. Nevertheless, it will be shown in this work that, for fuel rich combustion conditions, there may be situations where chemical equilibrium is not attained even for relatively large residence times. It seems that, in such conditions, the large variety of chemical time scales of combustion could lead to non-equilibrium phenomena similar to the classical ones, such as thermal NO formation involving multi-step chemical reactions.

To the best of our knowledge, PSRs have not been comprehensibly analyzed yet in conditions relevant to soot formation, i.e., fuel rich combustion conditions. It is interesting to study then the PSRs behavior under such conditions, as soot formation is important for various reasons. For instance, in some practical combustion systems, such as furnaces for industrial applications, the intermediate formation of soot is desirable due to it enhances the radiative heat transfer (Bockhorn, 1994). If not properly oxidized however, before releasing it into the environment, the soot formed may have hazardous effects on human health (Vovelle, 2000; Flagan and Seinfeld, 2012). Accordingly, in this

work, the origins of non-equilibrium phenomena observed in PSRs, for relatively large reactor residence times, burning fuel rich hydrocarbon/air mixtures, are described and discussed. More specifically, such phenomena is characterized here using a simple CO/O2 system. The final part of the work highlights some of the main conclusions drawn from the results obtained. A short exploration of the PSR non-equilibrium behavior using more complex mixtures such as syngas/O2 ones is also included.

2 Methodology

In this work, all PSR simulations are performed considering two separate inlet streams, one involving CO (or syngas) as fuel, and the other involving O2 as oxidant, both at 300 K and 1 atm. Furthermore, all PSR-related computations are carried out considering adiabatic conditions and using Chemkin II routines (Kee et al., 1991). More specifically, reaction processes are modeled using Arrhenius laws and integrated using SUNDIALS/CVODE (SUNDIALS, 2016). Equilibrium computations are in turn performed using STANJAN (Lutz et al., 1996).

Accordingly, in order to define the appropriate reactor residence time range to be studied, a preliminary analysis of PSR results, obtained for mixture equivalence ratios ranging from 1 to 5, as a function of residence time, is first carried out.

The PSR non-equilibrium phenomena observed under fuel rich conditions, for relatively large reactor residence times, is then characterized using a simple CO/O2 system, involving four (4) chemical species and three (3) reaction steps (Gardiner Jr., 2000) – specific details of the associated CO/O2 kinetic mechanism utilized are provided in Table 1. The referred characterization is emphasized by considering three different reactor residence times, namely 50, 100 and 200 ms.

Table 1. CO/O2 mechanism (Gardiner Jr., 2000) ($k = AT^b exp(-E/RT)$, $A: mole - cm - K$, $E: cal/mole$).

ID	Reaction	A	b	E
R1	CO + O2 ⇌ CO2 + O	1.260E+13	0.0	23682.94
R2	CO + O + M ⇌ CO2 + M	1.540E+15	0.0	1510.70
R3	O + O + M ⇌ O2 + M	5.400E+13	0.0	-899.69

(') R1 and R2 third body efficiencies: O2/0.4/ CO/0.75/ CO2/1.5/

The results obtained for the simple CO/O2 mechanism are extended such as to cover a more complex fuel/oxidant mixture involving syngas and O2. For the sake of simplicity, syngas is modelled here as an equimolar mixture of CO and H2. The kinetic mechanism used to describe the combustion of syngas/O2 is the widely used GRI-Mech 3.0 (GRI-Mech, 2016), which involves 53 chemical species and 325 reaction steps. The same PSR conditions are used in both CO/O2 and syngas/O2 mixtures.

Following the presentation of the non-equilibrium related results, and based on the simple CO/O2 mechanism given in Table 1, the origins of the PSR non-equilibrium phenomena is elucidated next. This is done by (i) analyzing the relevance of the reaction steps; (ii) deriving and assessing analytical expressions, which reproduce the PSR results; and (iii) examining asymptotic limit solutions emphasizing a possible cause of the non-equilibrium behavior observed. In addition, further syngas/O2 mixture-related results are discussed to underscore the extent of the non-equilibrium present in PSR simulations under fuel rich conditions (Appendix section).

3 Results and discussion

The main results obtained in this work are presented and discussed in this section.

3.1 PSR temperature and residence time

The classical response of PSRs, in terms of temperature as a function of reactor residence time, is illustrated in Fig. 1, which shows CO/O2 and syngas/O2 results for mixture equivalence ratios (ϕ) between 1 and 5. Two particular aspects to be observed in this figure relate to the characteristic times required to attain both the temperature plateaux/invariances and the PSR extinction conditions. On one hand, when the temperature change tends to zero as the residence time increases, it could be presumed that the chemical equilibrium has been attained. Such an assumption is always valid for a PSR controlled by a single Arrhenius reaction (Zeldovich et al., 1985). The other end of the curves shown in Fig. 1 highlights, on the other hand, the reactor extinction characteristic time. Classically, both characteristic equilibrium and extinction times are sensitive to the mixture equivalence ratio. Similarly, it is seen from Fig. 1 that, as ϕ

increases departing form stoichiometry, the residence time required to attain the temperature plateau/invariance increases as well. For instance, considering the syngas/O2 results, for $\phi = 1$, the temperature plateau is reached around 1 ms; whereas for $\phi = 3$, this time is 30 ms, approximately.

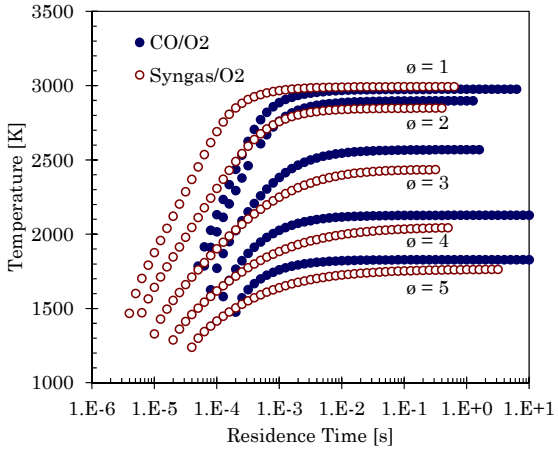

Fig. 1. PSR temperature as function of residence time, characterizing CO/O2 and Syngas/O2 mixtures, for ϕ = 1, 2, 3, 4 and 5.

Following the results shown in Fig. 1, a reactor residence time equal to 100 ms has been chosen for the main analyses carried out in this work. Notice that, in the range of equivalence ratios studied, this value is orders of magnitude beyond the characteristic time that CO/O2 mixtures require to reach the temperature plateau. A similar behavior is observed in the case of the syngas/O2 mixtures (see Fig. 1), even though for $\phi > 4$ this value of residence time (100 ms) is now closer to the corresponding characteristic time required for reaching the plateau. In addition to this value of residence time, the results corresponding to two other values, namely 50 and 200 ms, i.e., half and twice this time, have been also analyzed. Accordingly, the PSR non-equilibrium characteristics under discussion here have been emphasized for three different residence times, as detailed in the following section.

3.2 Non-equilibrium characteristic behavior

Consider initially the combustion of CO/O2 mixtures only, for the sake of argument, corresponding to the selected residence times of 50, 100 and 200 ms. In this case, by examining the curves of Fig. 1, it can be seen that, at these selected times, the reactor

temperature no longer varies with residence time. Therefore, the conditions characterizing the PSR could be presumed to correspond to those associated with chemical equilibrium. Equilibrium concentrations are found to occur indeed for two of the four chemical species present in the CO/O2 mechanism utilized, namely CO and CO2. The same occurs in the case of both the reactor temperature, directly related to the heat release, and the reactor entropy. More specifically, as illustrated in Fig. 2, which compares equilibrium and PSR results associated with temperature and entropy, both the reactor temperature and the reactor entropy values closely follow the chemical equilibrium corresponding ones. This is particularly true for the range of fuel rich mixture equivalence ratios studied.

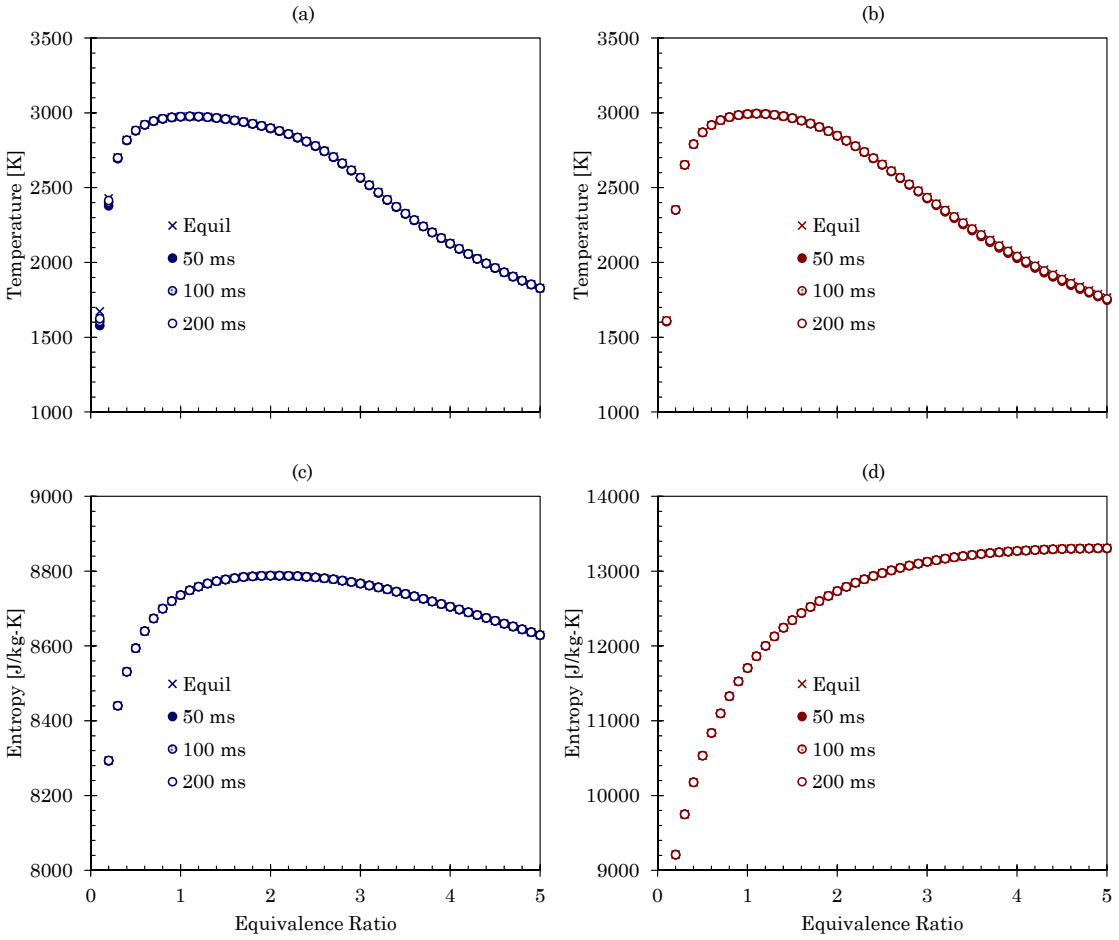

Fig. 2. Equilibrium/PSR temperature (top) and entropy (bottom) as a function of mixture equivalence ratio for residence times equal to 50, 100 and 200 ms, (a) & (c) CO/O2, (b) & (d) Syngas/O2.

Nevertheless, for equivalence ratios beyond 3, approximately, equilibrium concentrations do not prevail for the other two chemical species, O2 and O. This aspect may be verified in Fig. 3 left plots, which compare chemical equilibrium and PSR molar

fractions results associated with O2 (top plots) and O (bottom plots), as a function of the mixture equivalence ratio. More specifically, a significant departure from equilibrium may be seen in Fig. 3 top left plot, with O2 molar fractions that are up to three orders of magnitude larger than the equilibrium values. Notice that the increase in residence time slightly delays the appearance of the non-equilibrium O2 and O features only, but the observed trends are not affected.

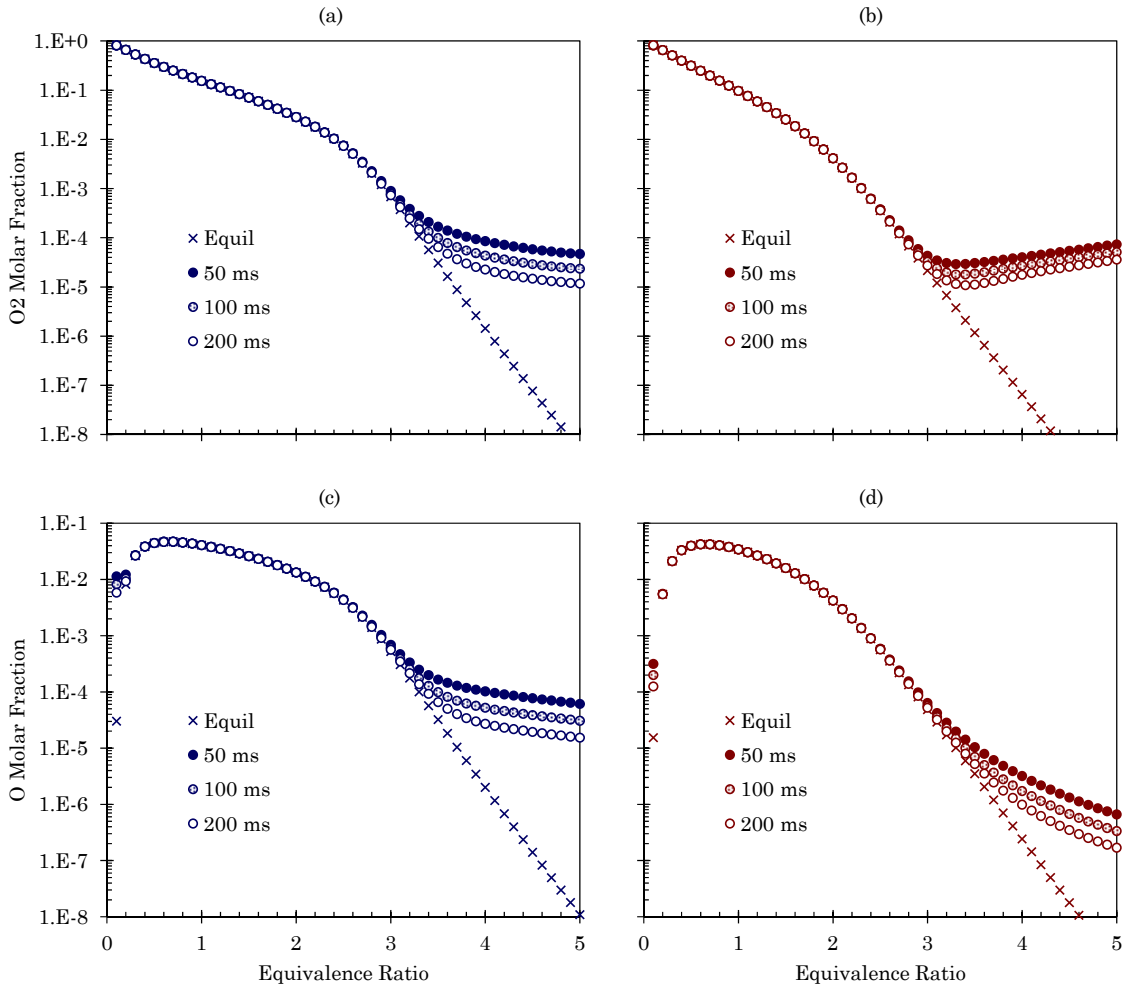

Fig. 3. Equilibrium/PSR O2 (top) and O (bottom) molar fractions as a function of mixture equivalence ratio for residence times equal to 50, 100 and 200 ms, (a) & (c) CO/O2, (b) & (d) Syngas/O2.

A somewhat similar scenario is observed in the case involving the combustion of syngas/O2 mixtures, Fig. 3 right plots. Indeed the observed non-equilibrium phenomena are also present when larger kinetic mechanisms, such as the widely used GRI-Mech 3.0 (GRI-Mech, 2016), are employed. It should be underscored that in this case the O2 molar fraction departures from equilibrium increase with the increase in equivalence ratio. It is

worth emphasizing that the GRI-Mech mechanisms have been considered as the basis for the developing of more complex kinetic mechanisms (Appel et al., 2000; D'Anna, 2008), tailored for specific purposes such as soot formation. The significance of the findings described in this section may vary depending of the context in which PSRs are utilized. Since O2 is usually considered as a soot oxidizing species (Lindstedt, 1994), when soot formation modelling is of interest, for instance, the larger O2 non-equilibrium concentration could lead to a significantly smaller amount of soot formed, when compared to that resulting from considering the O2 equilibrium values. Therefore, O-related species results coming from PSR simulations at relatively high equivalence ratios need to be carefully assessed.

3.3 Origins of non-equilibrium behavior

In this section, considering the value of 100 ms for the reactor residence time, the origins of the non-equilibrium phenomena identified above are analyzed. Departing from the simple CO/O2 mechanism given in Table 1, the relevance of the reaction steps characterizing this kinetic mechanism is thus first discussed. This is followed by the derivation of analytical expressions that reproduce the PSR results obtained. Finally, asymptotic limit solutions are analyzed to emphasize a possible cause of the non-equilibrium behavior observed at high equivalence ratios.

3.3.1 Relevance of reaction steps

Classically (Turns, 2000), for a system involving N chemical species and L reaction steps, the (net) rate of production, $\dot{\omega}_j$, of the j^{th} species, X_j, is given by,

$$\dot{\omega}_j = \sum_{i=1}^{L} \left(v''_{ji} - v'_{ji}\right) q_i \,, \qquad j = 1, \dots, N, \tag{1}$$

where

$$q_i = k_{if} \prod_{j=1}^{N} \left[X_j\right]^{v'_{ji}} - k_{ib} \prod_{j=1}^{N} \left[X_j\right]^{v''_{ji}}, \qquad i = 1, \dots, L. \tag{2}$$

In these equations, q_i is the rate of progress variable for the i^{th} elementary reaction. Additionally, v'_{ji} and v''_{ji} stand for the stoichiometric coefficients on the reactants (left) and

products (right) side of the reactions, respectively; whereas k_{if} and k_{ib} are, respectively, the forward and backward reaction rate constants, functions of temperature (primarily). $[X_j]$ denotes in turn molar concentration of species X_j. Note that for the sake of simplicity the third body efficiencies are not accounted for.

Accordingly, for the simple CO/O2 mechanism used in this work (Table 1), featuring 4 chemical species (plus the third body M) and 3 reaction steps, the rate of progress variables, q_i, are expressed as follows,

$$q_1 \equiv q_{1f} - q_{1b} = k_{1f}[CO][O_2] - k_{1b}[O][CO_2], \tag{3}$$

$$q_2 \equiv q_{2f} - q_{2b} = k_{2f}[CO][O][M] - k_{2b}[CO_2][M], \tag{4}$$

$$q_3 \equiv q_{3f} - q_{3b} = k_{3f}[O][O][M] - k_{3b}[O_2][M], \tag{5}$$

so that the reaction rates are given by,

$$\dot{\omega}_{CO} = -q_1 - q_2, \tag{6}$$

$$\dot{\omega}_{O_2} = -q_1 + q_3, \tag{7}$$

$$\dot{\omega}_{O} = q_1 - q_2 - 2q_3, \tag{8}$$

$$\dot{\omega}_{CO_2} = q_1 + q_2. \tag{9}$$

The rate of progress variable trends, associated with each of the three reaction steps characterizing the CO/O2 mechanism utilized – Eqs. (3)-(5), obtained from PSR simulations, are shown in Fig. 4. For the sake of argument, the discussion of Fig. 4 right plot results will be postponed to Section 3.3.3 below. Focusing then on Fig. 4 left plot results, it is readily seen that the rate of progress variable q_3, which corresponds to the CO/O2 mechanism third reaction (R3), is several orders of magnitude smaller than q_1 and q_2. This is particularly true when mixture equivalence ratios beyond 3 are considered. The relatively small value of q_3 implies that the R3 contribution to the chemical species productions rates could be neglected. This last aspect is emphasized in Fig. 5, which shows O2 and O production rates, total and discriminated according to each of the reactions composing the CO/O2 mechanism, as a function of equivalence ratio.

Indeed, Fig. 5 shows that the O2 and O production rates associated with R3 is nearly zero for almost all rich equivalence ratios studied. Consequently, the total O2 and O

production rates are found to be independent of R3 contributions. More specifically, the O2 rate of production essentially corresponds to that coming from R1 (Fig. 5a); whereas the O rate of production represents mainly the sum of R1 and R2 contributions (Fig. 5b). This implies in practice that, if R3 is removed from the CO/O2 mechanism or its contribution is neglected ($q_3 \rightarrow 0$), both O2 and O production rates within the PSR will not be significantly affected. Accordingly, the O2 and O production rates, Eqs. (7) and (8), can be rewritten as follows,

$$\dot{\omega}_{O_2} \approx -q_1, \tag{10}$$

$$\dot{\omega}_O \approx q_1 - q_2, \tag{11}$$

Therefore, Eqs. (10) and (11) will be used in the following section when deriving analytical expressions characterizing the PSR behavior.

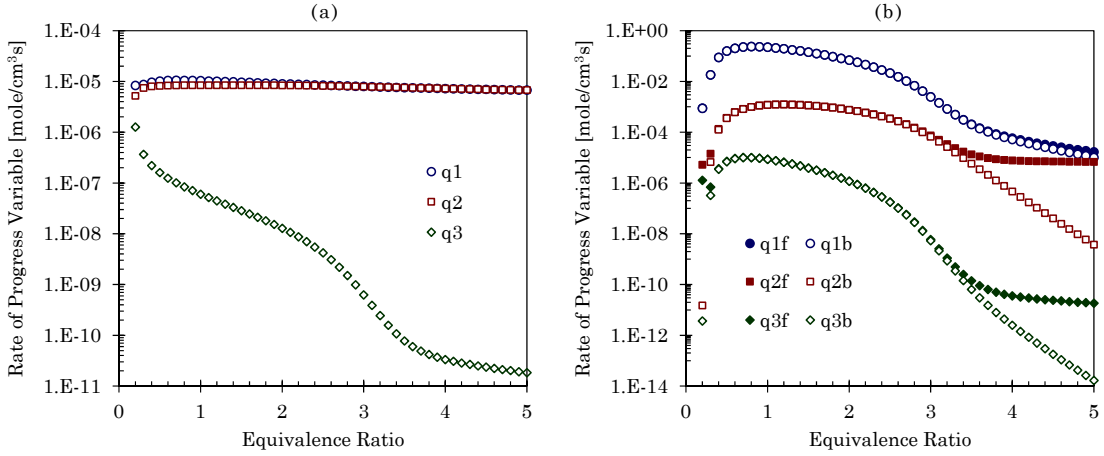

Fig. 4. Rate of progress variable as a function of equivalence ratio, (a) full and (b) forward/backward components – CO/O2 mixtures.

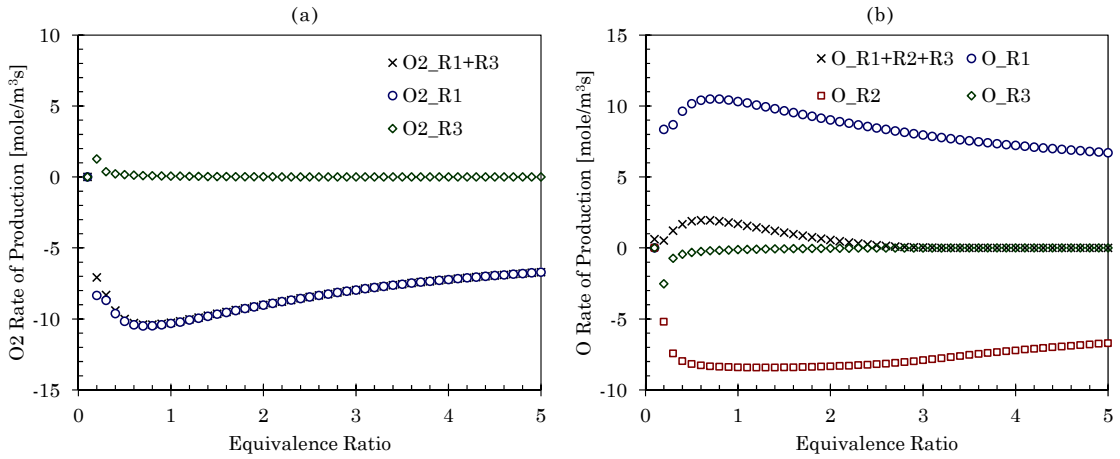

Fig. 5. Chemical species production rates as a function of equivalence ratio, (a) O2 and (b) O – CO/O2 mixtures.

3.3.2 Analysis of the PSR behavior

In order to gain an insight about the PSR non-equilibrium response at relatively high equivalence ratios, analytical expressions aiming to reproduce the PSR results are derived in this section. Accordingly, for a PSR at steady state, the rate of production $\dot{\omega}_j$ is given by (Glassman and Yetter, 2008),

$$\dot{\omega}_j = \frac{1}{\left(\frac{\rho V}{\dot{m}}\right)}\left(\frac{\rho}{\bar{W}_j}Y_j - \frac{\rho}{\bar{W}_j}Y_{j,0}\right); \tag{12}$$

which, using the definitions of reactor mean residence time ($\tau_r = \rho V/\dot{m}$) and molar concentration ($[X_j] = \rho Y_j/\bar{W}_j$), can be expressed as,

$$\dot{\omega}_j = \frac{1}{\tau_r}\left\{[X_j] - [X_j]_0\right\}. \tag{13}$$

In Eqs. (12) and (13), Y_j represents species mass fraction, $\bar{W}_j$ species molecular weight, ρ density, $\dot{m}$ reactor mass flow rate, V reactor volume, and the subscript 0 indicates reactor inlet conditions.

Following Eq. (13) then, the O2 and O production rates within the PSR are given by,

$$\dot{\omega}_{O_2} = \frac{1}{\tau_r}\{[O_2] - [O_2]_0\}, \tag{14}$$

$$\dot{\omega}_O = \frac{1}{\tau_r}\{[O] - [O]_0\} = \frac{1}{\tau_r}\{[O]\}, \qquad ([O]_0 = 0). \tag{15}$$

Thus, from equating Eq. (10) and (14), as well as Eq. (11) and (15), two expressions relating $[O_2]$ and $[O]$ are obtained,

$$\dot{\omega}_{O_2} \approx -q_1 = -k_{1f}[CO][O_2] + k_{1b}[O][CO_2] = \frac{1}{\tau_r}\{[O_2] - [O_2]_0\}, \tag{16}$$

$$\begin{aligned} \dot{\omega}_O \approx q_1 - q_2 = k_{1f}[CO][O_2] - k_{1b}[O][CO_2] - k_{2f}[CO][O][M] \\ + k_{2b}[CO_2][M] = \frac{1}{\tau_r}\{[O]\}. \end{aligned} \tag{17}$$

Finally, solving Eqs. (16) and (17) for $[O]$ leads to,

$$\begin{aligned} \frac{\left\{\frac{1}{\tau_r} + k_{1f}[CO]\right\}[O_2] - \frac{1}{\tau_r}\{[O_2]_0\}}{k_{1b}[CO_2]} \\ = \frac{\{k_{1f}[CO]\}[O_2] + k_{2b}[CO_2][M]}{\frac{1}{\tau_r} + k_{1b}[CO_2] + k_{2f}[CO][M]}; \end{aligned} \tag{18}$$

or, rewriting conveniently this equation in order to perform an order of magnitude analysis, to

$$\frac{\{a+b\}[O_2] - c}{d} = \frac{b[O_2] + e}{a + d + f}. \tag{19}$$

Accordingly, the analytical expressions that allow computing $[O_2]$ and $[O]$ are,

$$[O_2] = \frac{\{c\} + \left\{\frac{de}{(a+d+f)}\right\}}{\{a+b\} - \left\{\frac{bd}{(a+d+f)}\right\}}, \tag{20}$$

$$[O] = \frac{\{a+b\}[O_2] - \{c\}}{\{d\}}. \tag{21}$$

Notice that in Eqs. (19)-(21), the coefficients a to f are given by,

$$\begin{aligned} a = \frac{1}{\tau_r}, \qquad b = k_{1f}[CO], \qquad c = \frac{1}{\tau_r}\{[O_2]_0\}, \qquad d = k_{1b}[CO_2], \\ e = k_{2b}[CO_2][M], \qquad f = k_{2f}[CO][M]. \end{aligned} \tag{22}$$

In order to use Eqs. (20) and (21) to obtain the O2 and O molar concentrations, the values of coefficients a to f need to be determined. Indeed, coefficients a to f are presumed to be known at PSR steady state conditions. More specifically, (i) τ_r is a specified reactor parameter, 100 ms in this particular case; (ii) the O2 molar concentration at the reactor inlet $[O_2]_0$ is a known function of equivalence ratio; (iii) the forward and backward reaction rate constants k_{if} and k_{ib} are functions of temperature, which is assumed to correspond to the equilibrium one; and (iv) the CO and CO_2 molar concentrations are supposed to correspond to their equilibrium values, i.e., $[CO] = [CO]_e$ and $[CO_2] = [CO_2]_e$.

The O2 and O molar fractions corresponding to the analytical expressions given in Eqs. (20) and (21) are shown in Fig. 6 as a function of mixture equivalence ratio. As it may be readily noticed from this figure, both expressions reproduce quite well the O2 and O PSR results. This means that, similarly to the full PSR results, the analytical ones also deviate from the corresponding equilibrium values for equivalence ratios beyond 3, approximately. Even though they are not shown here for the sake of brevity, the same trends are obtained for the other two investigated residence times, namely 50 and 200 ms. In the following section, Eqs. (20) and (21) will be used to identify a possible cause for the referred O2 and O deviations from chemical equilibrium.

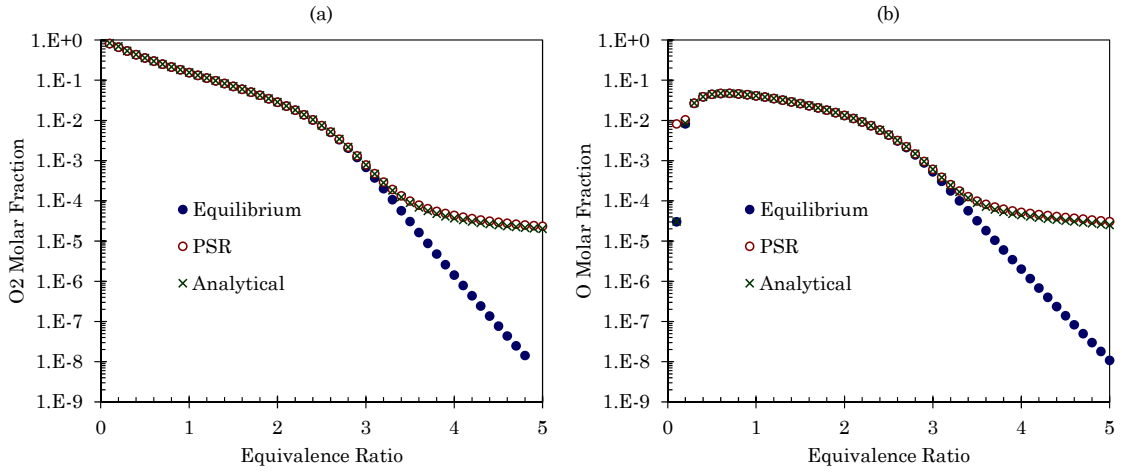

Fig. 6. Chemical species molar fractions as a function of equivalence ratio characterizing equilibrium conditions, along with both the full PSR and the analytical solutions, (a) O2 and (b) O – CO/O2 mixtures.

3.3.3 Asymptotic limit solutions

In this section, the analytical expressions given in Eqs. (20)-(21) are used to identify a possible reason why, even if they follow the corresponding equilibrium values up to a given mixture equivalence ratio (about 3 in this case), the O2 and O PSR results deviate from equilibrium further on. In order to do so, order of magnitude analyses of the different terms appearing within the braces in the right hand side of Eq. (20) have been carried out. The results from such analyses are summarized in Fig. 7 left (numerator-related) and right (denominator-related) plots. Starting from Fig. 7 right plot, it is possible to see that, even when they have a similar order of magnitude, the term $\{a+b\}$ is slightly larger than the $\{bd/(a+d+f)\}$ one, which always yields a positive result when the latter is subtracted from the former. Notice as well from Fig. 7b that the result from the referred subtraction, $\{a+b\}-\{bd/(a+d+f)\}$, varies essentially monotonically with equivalence ratio; and that there is no abrupt change in its trend at equivalence ratio around 3, i.e., where the O2 and O deviations from equilibrium appear.

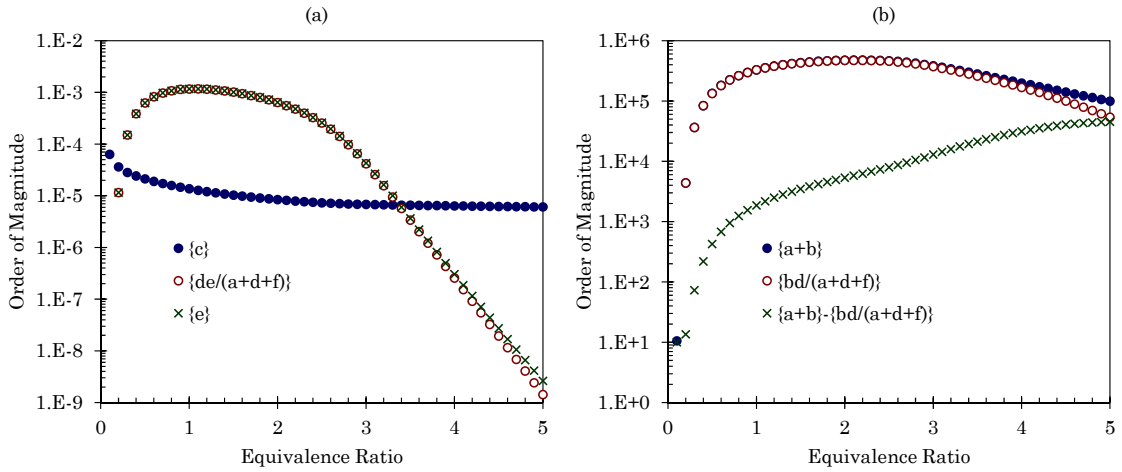

Fig. 7. Order of magnitude of parameters appearing in Eq. (20) right hand side, (a) numerator- and (b) denominator-related terms.

Considering now the results shown in Fig. 7 left plot, it may be first noticed that, for the range of equivalence ratios studied, the second term appearing in the numerator of Eq. (20) right hand side, $\{de/(a+d+f)\}$, can be reasonably approximated by coefficient e, as they have roughly the same values, i.e., $(a+f) \ll d$. Therefore, in the analyses performed, instead of referring directly to the term $\{de/(a+d+f)\}$, references to coefficient e are carried out. It may be clearly seen in Fig. 7a as well that the first term

appearing in the numerator of Eq. (20) right hand side, coefficient c, which relates to the PSR prescribed conditions, remains almost constant (according to the semi-log scale utilized) in the fuel rich equivalence ratio range. Nevertheless, the values of coefficient e decreases by six orders of magnitude from equivalence ratio 1 to 5. Such a decrease is directly related to the large activation energy E_{2b}, which leads to a large decrease of k_{2b} when the equilibrium temperature decreases with ϕ. Furthermore, for equivalence ratios below 3, $c = \{[O_2]_0\}/\tau_r \ll e = k_{2b}[CO_2][M]$, essentially. For equivalence ratios higher than this limiting value (~3) however, the opposite is observed. Accordingly, since the O2 and O molar fractions deviations from equilibrium appear at an equivalence ratio of about 3 (Fig. 6), it seems that the relationship between the c and e values, i.e., how they compare to each other, plays a key role in the referred deviations from equilibrium, observed for high equivalence ratios.

In order to further emphasize the relationship between coefficients c and e and its influence on the deviations from chemical equilibrium, departing from Eqs. (20) and (21), two limiting situations are examined,

$$c \ll e \rightarrow [O_2] = \frac{\{e\}}{\{a+b\} - \left\{\frac{bd}{(a+d+f)}\right\}}, \qquad [O] = \frac{\{a+b\}[O_2]}{\{d\}}, \tag{23}$$

$$c \gg e \rightarrow [O_2] = \frac{\{c\}}{\{a+b\} - \left\{\frac{bd}{(a+d+f)}\right\}}, \qquad [O] = \frac{\{a+b\}[O_2] - \{c\}}{\{d\}}. \tag{24}$$

The analytical solutions corresponding to these two limit situations, along with equilibrium- and PSR-related results are shown in Fig. 8. The trends of the asymptotic limit solutions given in this figure confirm that when $c \gg e$ the PSR deviations from equilibrium become significant. In other words, it seems that beyond a certain equivalence ratio, the decrease in equilibrium temperature is such that the backward reaction rate of the CO/O2 mechanism second reaction becomes unimportant, and the oxides composition within the PSR is controlled by the residence time. This last aspect can be also visualized in Fig. 4b, which highlights how the difference between the q_2

forward and backward components gets progressively larger from the point where the O2 and O molar fractions deviations start. Furthermore, as it may be expected from the definition of the c coefficient, the onset of non-equilibrium effects is inversely proportional to the residence time. Reducing the residence time leads therefore to non-equilibrium effects appearing at smaller equivalence ratios (Fig. 3). From Fig. 8 results it follows then that one way of avoiding the equilibrium departures would involve ensuring that the c coefficient is always relatively small when compared to e.

Finally, it is worth noticing that the point made in this work relates to fact that, even when the reactor is operating in the region of the temperature plateau (see Fig. 1), where chemical equilibrium conditions could be presumed, there are chemical species such as O2 and O, whose molar fractions do not correspond to those ones characterizing equilibrium. The findings described here bring attention thus to PSR results, obtained at relatively high mixture equivalence ratios, which may not correspond to their equilibrium counterparts in situations where it could be expected to happen so.

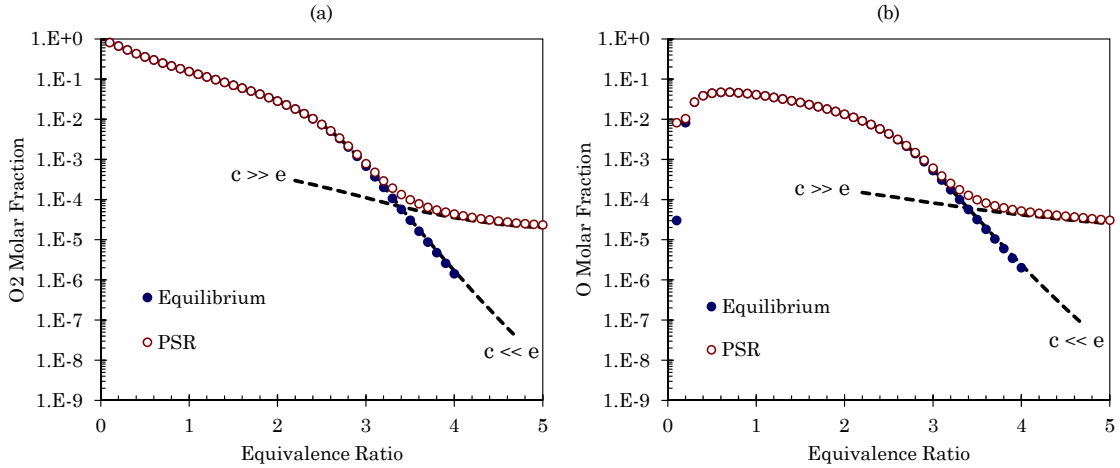

Fig. 8. Chemical species molar fractions as a function of equivalence ratio characterizing equilibrium and PSR conditions, along with two asymptotic limit solutions, (a) O2 and (b) O – CO/O2 mixtures.

4 Conclusions

In this work, the origins of non-equilibrium behavior observed in PSRs, for relatively large residence times, burning fuel rich mixtures, have been studied. In order to do so, an analysis of PSR temperatures obtained for five different mixture equivalence ratios, as a function of residence time, has been firstly carried out. The referred PSR deviations from

chemical equilibrium have been then characterized using a simple CO/O2 system. The origins of such non-equilibrium behavior have been elucidated by (i) analyzing the relevance of the reaction steps, (ii) deriving and assessing analytical expressions reproducing the PSR results, and (iii) examining asymptotic limit solutions emphasizing a possible cause of the non-equilibrium behavior observed.

The main results point out that the PSR non-equilibrium behavior is controlled by a competition between (i) the rate of progress variable backward component of the CO + O + M ⇌ CO2 + M reaction, and (ii) the ratio between the reactor inlet O2 molar concentration and the reactor residence time. This backward reaction rate dramatically decreases with temperature, thus leading to a direct proportionality between the O2 concentration and the corresponding inlet value. Therefore, even when the reactor is operating in a region of temperature invariance (plateau), where chemical equilibrium conditions could be presumed, there are some chemical species, whose molar fractions significantly depart from chemical equilibrium. This same scenario is observed when both simple and large kinetic mechanisms are utilized. In order to emphasize this point, the extent of the non-equilibrium present in PSR simulations under fuel rich conditions has been underscored by discussing results obtained for syngas/O2 mixtures, some of which are given in the Appendix section. It is believed that the chain-termination reaction CO + OH ⇌ CO2 + H, which responds for almost all CO to CO2 conversion and hence controls the rate of heat release (temperature), is partially responsible for the particular results obtained in this case. Notice that for this reaction, the reverse path activation energy is very large when compared to the direct one.

It is concluded then that particular attention should be paid when analyzing PSR results, obtained at relatively high mixture equivalence ratios, which may not correspond to their equilibrium counterparts, in situations where it could be expected to happen so. It remains unclear at this point whether such non-equilibrium effects are an artifact of the chemical kinetics mechanism that should be corrected or if they could be experimentally verified.

5 Acknowledgments

This work has been supported by Petrobras under the technical monitoring of Dr. Ricardo Serfaty (Project: Development of a modeling technique for turbulent combustion

based on an Eulerian/Lagrangian approach – Phase II, Contract No.: 0050.0080122.12.9). During this work Luís Fernando Figueira da Silva was on leave from the Institut Pprime (Centre National de la Recherche Scientifique, France).

6 Appendix

What makes the previous discussion even more relevant is that the PSR non-equilibrium issue addressed is also present when other more complex or detailed chemical kinetic mechanisms are utilized. As shown in Fig. 3b and d for instance, deviations from chemical equilibrium appear as well when the GRI-Mech 3.0 (GRI-Mech, 2016) mechanism is used to describe the combustion of syngas/O2 mixtures. Since in these more detailed kinetic mechanisms there are chemical species other than those four ones present in the CO/O2 mechanism (CO, O2, O and CO2), it may be anticipated that some of these other chemical species are also characterized by a non-equilibrium behavior. This happens indeed in the case of the syngas/O2 mixtures considered in this work. For instance, Fig. 9 shows equilibrium and PSR results associated with H and OH molar fractions characterizing the syngas/O2 mixtures combustion. It may be promptly seen from this figure that, even when the temperature characterizing the PSR steady state operation follows the chemical equilibrium temperature (Fig. 2b), the PSR H and OH molar fraction values do not accompany the corresponding equilibrium ones.

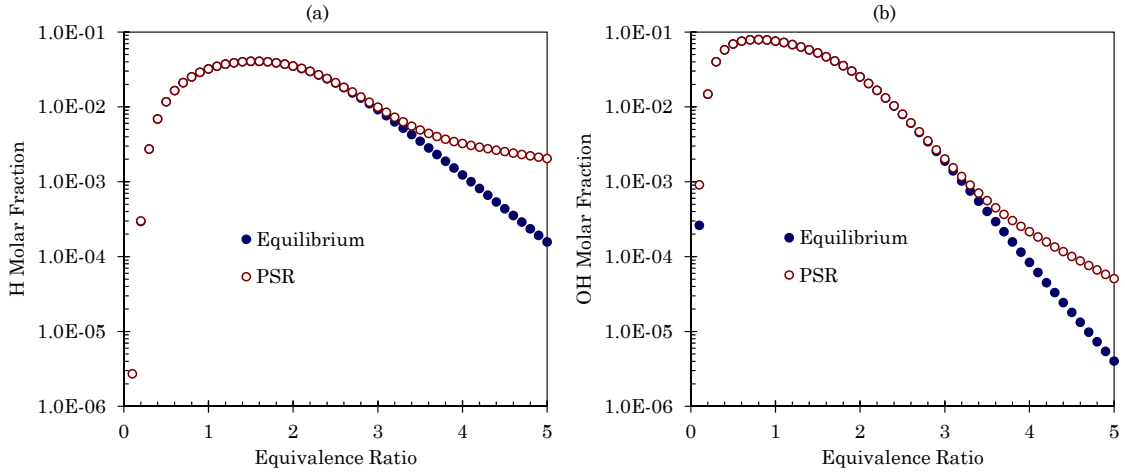

Fig. 9. Selected syngas/O2 characteristic parameters as a function of equivalence ratio, (a) H and (b) OH molar fractions.

Indeed, from the twelve chemical species computed in both equilibrium and PSR calculations, only two of them, H and H2, do not involve oxygen as one of its constituents. More specifically, H2 results correspond to those associated with chemical equilibrium, whereas H molar fractions deviate from equilibrium as shown in Fig. 9a. The remaining ten chemical species are oxygenated species. From these species, only three of them, CO, CO2 and H2O, attain equilibrium concentrations. Notice that as it happens for the CO/O2 mechanism CO is also in equilibrium in this case. The equilibrium values of the other two species (CO2 and H2O) can be considered as expected results, since they represent major species in all hydrocarbon combustion processes. In turn, the molar fractions of the other seven oxygenated species, namely, O2 (Fig. 2b), O (Fig. 2d), OH (Fig. 9b), HO2, H2O2, HCO and CH2O, deviate from their equilibrium values.

The results described in this section confirm the fact that, depending on the reactions controlling the combustion process, deviations from equilibrium of several chemical species occur. In other words, their PSR molar fractions at relatively high equivalence ratios do not correspond to those ones obtained from chemical equilibrium calculations. These findings emphasize of course the need of carefully using PSR results coming from relatively high equivalence ratio-based simulations, where it could be presumed that chemical equilibrium conditions prevail.

7 References

Adhikari, S., Sayre, A. and Chandy, A. J. 2016. A hybrid Newton/time integration approach coupled to soot moment methods for modeling soot formation and growth in perfectly stirred reactors, *Combustion Science and Technology*. [Online]. Available from - http://www.tandfonline.com/doi/abs/10.1080/00102202.2016.1177035. [Accessed: 23rd May 2016].

Amzin, S. and Cant, R. S. 2015. Assessment of an equivalent reaction networks approach for premixed combustion. *Combustion Science and Technology* 187 (11), p. 1705-1723.

Appel, J., Bockhorn, H., Frenklach, M. 2000. Kinetic modeling of soot formation with detailed chemistry and physics: laminar premixed flames of C2 hydrocarbons, *Combustion and Flame* 121 (1-2), p. 122-136.

Bockhorn, H. (ed.) 1994. *Soot Formation in Combustion, Mechanisms and Models*. Berlin: Springer-Verlag.

Celis, C., Moss, B. and Pilidis, P. 2009. *Emissions modelling for the optimisation of greener aircraft operations*. In Proceedings of the ASME Turbo Expo 2009, Volume 2: Combustion, Fuels and Emissions. Orlando, USA, June 8-12. p. 167-178.

D'Anna, A. 2008. Detailed kinetic modeling of particulate formation in rich premixed flames of ethylene, *Energy & Fuels* 22 (3), p. 1610-1619.

De Toni, A., Hayashi, T. and Schneider, P. 2013. A reactor network model for predicting NOx emissions in an industrial natural gas burner. *Journal of the Brazilian Society of Mechanical Sciences and Engineering* 35 (3), p. 199-206.

Fichet, V., Kanniche, M., Plion, P. and Gicquel, O. 2010. A reactor network model for predicting NOx emissions in gas turbines. *Fuel* 89 (9), p. 2202-2210.

Flagan, R. C. and Seinfeld, J. H. 2012. *Fundamentals of Air Pollution Engineering*. New York: Dover Publications Inc.

Gardiner Jr., W. C. (ed.) 2000. *Gas-phase combustion chemistry*. New York: Springer.

Glassman, I. and Yetter, R. A. 2008. *Combustion*. 4th Ed. London: Academic Press.

GRI-Mech. 2016. *Welcome to the GRI-Mech Home Page!.* [Online] Available from: http://www.me.berkeley.edu/gri-mech/. [Accessed 23rd May 2016].

Kee, R. J., Rupley, F. M. and Miller, J. A. 1991. *CHEMKIN II: A Fortran chemical kinetics package for the analysis of gas-phase chemical kinetics.* Technical Report, Sandia National Laboratories, Livermore, CA, USA.

Le Cong, T. and Dagaut, P. 2007. Kinetics of natural gas, natural gas/syngas mixtures oxidation and effect of burnt gas recirculation: Experimental and detailed modeling. In Proceedings of the ASME Turbo Expo 2007, Volume 1: Turbo Expo 2007. Montreal, Canada, May 14-17. p. 387-395.

Le Cong, T. and Dagaut, P. 2008. Experimental and detailed kinetic modeling of the oxidation of methane and methane/syngas mixtures and effect of carbon dioxide addition. *Combustion Science and Technology* 180 (10-11), p. 2046-2091.

Lindstedt, P. R. 1994. Simplified soot nucleation and surface growth steps for non-premixed flames. In: Bockhorn, H. (ed.) *Soot Formation in Combustion, Mechanisms and Models*. Berlin: Springer-Verlag.

Longwell, J. P. and Weiss, M. A. 1955. High temperature reaction rates in hydrocarbon combustion. *Industrial & Engineering Chemistry* 47 (8), p. 1634-1643.

Lutz, A. E., Rupley, F. M. and Kee, R. J. 1996. EQUIL: *A CHEMKIN Implementation of STANJAN, for Computing Chemical Equilibria.* Technical Report, Sandia National Laboratories. Livermore, CA, USA.

Mallampalli, H. P., Fletcher, T. H. and Chen, J. Y. 1998. Evaluation of CH4/NOx reduced mechanisms used for modeling lean premixed turbulent combustion of natural gas. *Journal of Engineering for Gas Turbines and Power* 120 (4), p.703-712.

Nikolaou, Z. M., Chen, J. Y. and Swaminathan, N. 2013. A 5-step reduced mechanism for combustion of CO/H2/H2O/CH4/CO2 mixtures with low hydrogen/methane and high H2O content. *Combustion and Flame* 160 (1), p. 56-75.

Orbegoso, E. M., Romeiro, C. D., Ferreira, S. B., and Figueira da Silva, L. F. 2011. Emissions and thermodynamic performance simulation of an industrial gas turbine. *Journal of Propulsion and Power* 27 (1), p. 78-93.

Snegirev, A. Yu. 2015. Perfectly stirred reactor model to evaluate extinction of diffusion flame. *Combustion and Flame* 162 (10), p. 3622-3631.

Snegirev, A. Yu. and Tsoy, A. S. 2015. Treatment of local extinction in CFD fire modeling. *Proceedings of the Combustion Institute* 35 (3), p. 2519-2526.

SUNDIALS. 2016. *SUNDIALS: SUite of Nonlinear and DIfferential/ALgebraic Equation Solvers*. [Online] Available from: http://computation.llnl.gov/casc/sundials/. [Accessed 23rd May 2016].

Sung, C. J., Law, C. K. and Chen, J. Y. 2001. Augmented reduced mechanisms for NO emission in methane oxidation. *Combustion and Flame* 125 (1-2), p. 906-919.

Turns, S. R. 2000. An introduction to combustion: concepts and applications. 2nd Ed. Singapore: McGraw-Hill.

Vovelle, C. (ed.) 2000. Pollutants from Combustion, Formation and Impact on Atmospheric Chemistry. Dordrecht: Springer.

Williams, F. A. 1985. *Combustion theory*. 2nd Ed. California: Benjamin Cummings.

Zeldovich, Ya. B., Barenblatt, G. I., Librovich, V. B. and Makhviladze, G. M. 1985. *The Mathematical theory of combustion and explosions*. New York: Consultants Bureau.